FULL PAPER

Dalton
www.rsc.org/dalton

A phenol–imidazole pro-ligand that can exist as a phenoxyl radical, alone and when complexed to copper(II) and zinc(II) †

Laurent Benisvy,*[a] Alexander J. Blake,[a] David Collison,[b] E. Stephen Davies,[a] C. David Garner,*[a] Eric J. L. McInnes,[b] Jonathan McMaster,*[a] Gavin Whittaker[c] and Claire Wilson[a]

[a] *School of Chemistry, The University of Nottingham, University Park, Nottingham, UK NG7 2RD. E-mail: Dave.Garner@nottingham.ac.uk*

[b] *Department of Chemistry, The University of Manchester, Oxford Road, Manchester, UK M13 9PL*

[c] *Department of Chemistry, The University of Edinburgh, West Mains Road, Edinburgh, UK EH9 3JJ*

Received 9th December 2002, Accepted 22nd January 2003
First published as an Advance Article on the web 23rd April 2003

A new *N*,*O*-bidentate, phenol–imidazole pro-ligand 2′-(4′,6′-di-*tert*-butylhydroxyphenyl)-4,5-diphenyl imidazole (LH) has been designed, synthesised, and characterised. LH possesses no readily oxidisable position (other than the phenol) and involves *o*- and *p*-substituents on the phenol ring that prevent radical coupling reactions. LH undergoes a reversible one-electron oxidation to generate the corresponding $[LH]^{\bullet+}$ radical cation that possesses phenoxyl radical character. The unusual reversibility of the $[LH]/[LH]^{\bullet+}$ redox couple is attributed, at least in part, to a stabilisation of $[LH]^{\bullet+}$ by intramolecular O–H ··· N hydrogen bonding. The compounds $[CuL_2]$ (**1**) and $[ZnL_2]$ (**2**) have been synthesised and characterised structurally, spectroscopically, and electrochemically. The crystal structures of **1**·4DMF, **1**·3MeOH, and **2**·2.5MeCN·0.3CH_2Cl_2 have been determined and each shown to possess an N_2O_2-coordination sphere, the geometry of which varies with the nature of the metal and the nature of the co-crystallised solvent. **1** and **2** each undergo two, reversible, ligand-based, one-electron oxidations, to form, firstly, $[M(L)(L^{\bullet})]^+$ and secondly $[M(L^{\bullet})_2]^{2+}$. The $[M(L)(L^{\bullet})]^+$ (M = Cu, Zn) cations have been generated by both electrochemical and chemical oxidation and their $[ML_2][BF_4]$ salts isolated as air-stable, dark green, crystalline solids. The UV/vis, EPR, and magnetic characteristics of these compounds are consistent with each cation involving an M^{II} (M = Cu or Zn) centre bound to a phenoxide (L^-) and a phenoxyl radical ($L^{\bullet}$). The structural information obtained by a determination of the crystal structures of $[CuL_2][BF_4]$·2CH_2Cl_2 and $[ZnL_2][BF_4]$·2CH_2Cl_2·0.75pentane fully supports this interpretation. For each of these salts, there is a clear indication that the coordinated phenoxyl radical is involved in intramolecular π–π stacking interactions that parallel those in galactose oxidase.

Introduction

Inspired by a knowledge of the nature of the catalytic centres of galactose oxidase (GAO)[1–3] and glyoxal oxidase (GLO)[4] a new *N*,*O*-bidentate pro-ligand, 2′-(4′,6′-di-*tert*-butylhydroxyphenyl)-4,5-diphenyl imidazole (LH) has been designed and synthesised.[5] LH involves the prospective donor groups *O*-phenol and *N*-imidazole that, respectively, resemble the tyrosine and histidine residues that coordinate Cu in GAO and GLO. To enhance the possibility of isolating complexes containing $L^{\bullet}$, HL contains no readily oxidisable functionality, other than the phenol group. The *ortho*- and *para*-^{t}Bu substituents inhibit pathways for the decomposition of the phenoxyl radical state and should stabilise this state by a positive inductive effect.

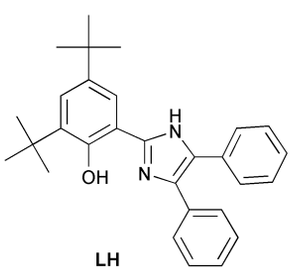

LH

† Based on the presentation given at Dalton Discussion No. 5, 10–12th April 2003, Noordwijkerhout, The Netherlands.

Experimental

$Cu(BF_4)_2$·H_2O, $Zn(BF_4)_2$·H_2O, $Ag[BF_4]$ and anhydrous MeOH were obtained from Aldrich Chemicals Ltd.; CH_2Cl_2 was freshly distilled from calcium hydride under dinitrogen.

Syntheses

LH. A mixture of 3,5-di-*tert*-butylhydroxybenzaldehyde (2 g, 8.8 mmol), benzil (1.8 g, 8.6 mmol), and ammonium acetate (5.2 g, 64 mmol) were refluxed for 2 h in glacial acetic acid (30 cm^3), during which time a yellow precipitate formed. An excess of de-ionised water (*ca.* 30 cm^3) was added to complete the precipitation. The crude product was collected by filtration, washed with water, and dried by suction. The resulting solid was dissolved in CH_2Cl_2 and dried over $MgSO_4$. The solution was filtered and the solvent was evaporated from the filtrate, to produce a pale yellow powder that recrystallised from CH_2Cl_2–pentane as a white cotton-wool-like solid in 75% yield (2.8 g). Single crystals of LH·Me_2CO were obtained by allowing a solution of LH in acetone to stand at −30 °C for one week; these crystals proved suitable for analysis by X-ray diffraction. Elemental analysis: calc. for $C_{29}H_{32}N_2O$: C 82.08, H 7.55, N 6.60; Found: C 81.63, H 7.64, N 6.58%. NMR (^{1}H, 300 MHz, $CDCl_3$): δ 13.2 (s, 1H, N–H), 9.23 (s, 1H, OH), 7.1–7.7 (m, 12H, ArH), 1.47 (s, 9H, ^{t}Bu), 1.62 (s, 9H, ^{t}Bu). NMR (^{13}C, 300 MHz, $CDCl_3$): δ 29.5, 31.6, 34.3, 35.3, 111.5, 117.3, 125.4, 125.9, 127.2, 128.4, 128.9, 130.7, 133.5, 135.2, 137.5, 140.3, 146.8, 154.5. Mp 283 °C. Positive EI-MS: ion at *m*/*z* 424 {M^+}. UV/vis

DOI: 10.1039/b212209j

(CH_2Cl_2): λ_{max}/nm (ε/M^{-1} cm^{-1}): 228 (26355), 277 (sh), 291 (20395), 321 (21480). IR (KBr pellet): 3426(s), 2961(s), 2903(s), 2864(s), 1605(m), 1584(mw), 1529(m), 1500(mw), 1475(s) cm^{-1}.

General procedure for the synthesis of [ML_2] compounds (M = Cu, Zn)

A solution containing LH (2 equivalents) dissolved in the minimum volume of MeOH was added to a solution of $M(BF_4)_2$·H_2O in MeOH (2–5 cm^3), The mixture was stirred at room temperature for 1 h, after which time an excess (a few drops) of Et_3N was added. After further stirring (1 h) the product was isolated and purified according to the particular procedure described below.

[Cu($L)_2$] (1). $Cu(BF_4)_2$·H_2O (301 mg, 1.18 mmol) in MeOH (5 cm^3) and LH (1 g, 2.36 mmol) in MeOH (200 cm^3) were reacted as described above. The resultant deep green solution was left to stand in air for 6 d at room temperature and brown–purple, rectangular, crystals of **1**·3MeOH were obtained. The crystals were collected by filtration, washed with MeOH, crushed, and dried *in vacuo*, affording a dark brown powder of **1** in 85% yield. Elemental analysis: calc. for $C_{58}H_{62}N_4O_2Cu$·2MeOH: C 73.96, H 7.19, N 5.75; Found: C 74.22, H 6.84, N 6.06%. Positive FAB-MS: ion at *m*/*z* 910 {M^+}. UV/vis (CH_2Cl_2): λ_{max}/nm (ε/M^{-1} cm^{-1}): 499 (670), 692 (550). Slow evaporation at room temperature of a solution of **1** in CH_2Cl_2–DMF (9 : 1) produced, after 3–6 d, orange block-like single crystals of **1**·4DMF.

[Zn($L)_2$] (2). $Zn(BF_4)_2$·H_2O (245 mg, 0.95 mmol) in MeOH (5 cm^3), LH (800 mg, 1.9 mmol) in MeOH (200 cm^3) were reacted as described above. The resultant colourless solution was allowed to evaporate at room temperature by exposure to air for 6 d and a white crystalline powder was obtained. This powder was collected by filtration, washed with MeOH, crushed and dried *in vacuo* to yield **2** as a white powder in 80% yield. Slow evaporation of a solution of **2** in CH_2Cl_2–MeCN (1 : 1) in air at room temperature produced colourless, lath-like, crystals of **2**·2.5MeCN·0.3CH_2Cl_2 after 2–4 d. Elemental analysis (of powdered **2**): calc. for $C_{58}H_{62}N_4O_2Zn$·2MeOH: C 73.82, H 7.17, N 5.74; Found: C 74.04, H 6.66, N 6.08%. Positive FAB-MS: ion at *m*/*z* 911 {M^+}.

General procedure for the synthesis of [ML_2][BF_4] compounds (M = Cu, Zn)

The reactions were carried out in pre-dried Schlenk vessels, in the absence of light, under an argon atmosphere, and using freshly distilled solvents. A solution of [ML_2] in CH_2Cl_2 was added to a suspension of Ag[BF_4] (1 eq.) in CH_2Cl_2 at −10 °C (ice/acetone bath). This caused the rapid formation of a silver mirror and an intense dark green coloured solution. The solution was stirred for 1 h at −10 °C, for 10 min at room temperature, and then filtered using a Teflon cannula equipped with a glass wool filter at one end (it was noted that the use of a *metallic* cannula induced a colour change of the solution and, therefore, was avoided). The solvent was evaporated under a reduced pressure to yield a dark coloured solid. Each product was purified according to the particular procedure described below.

[1][BF_4]. A solution of **1** (318 mg, 0.348 mmol) in CH_2Cl_2 (20 cm^3) and a suspension of Ag[BF_4] (68 mg, 0.348 mmol) in CH_2Cl_2 (5 cm^3) were reacted and the product isolated as described above. The resultant dark green solid was washed with freshly distilled Et_2O (2 × 30 mL) to remove any unreacted **1**. The solid was then dried under a reduced pressure to afford [**1**][BF_4] in 85% yield. Dark, block-shaped, single crystals of [**1**][BF_4]·2CH_2Cl_2 were grown by diffusion of hexane into a CH_2Cl_2 solution of **1**[BF_4] under an argon atmosphere at room temperature. Elemental analysis: calc. for $C_{58}H_{62}N_4O_2CuBF_4$·1CH_2Cl_2: C 65.52, H 5.92, N 5.18; Found: C 65.28, H 5.98, N 5.01%. Positive FAB-MS: ion at *m*/*z* 910 {M^+}.

[2][BF_4]. A solution of **2** (108 mg, 0.119 mmol) in CH_2Cl_2 (15 cm^3) and a suspension of Ag[BF_4] (23.2 mg, 0.119 mmol) in CH_2Cl_2 (5 cm^3) were reacted and the product isolated as described above. The green solid was dried under a reduced pressure and recrystallised by diffusion of hexane into a CH_2Cl_2 solution under an argon atmosphere at 4 °C. After one week microcrystalline dark-green, needle-like crystals of [**2**][BF_4] were obtained in 70% yield (~83 mg). Dark, block-like, single crystals of [**2**][BF_4]·2CH_2Cl_2·0.75pentane were obtained by diffusion of pentane into a CH_2Cl_2 solution of [**2**][BF_4] under an argon atmosphere at room temperature. Elemental analysis: calc. for $C_{58}H_{62}N_4O_2ZnBF_4$: C 69.71, H 6.21, N 5.60; Found: C 69.81, H 6.34, N 5.51%. Positive FAB-MS: ion at *m*/*z* 911 {M^+}.

Physical methods

Elemental analysis of the compounds isolated in these studies were carried out at the Microanalytical Laboratory of the School of Chemistry; University of Nottingham. FAB and EI mass spectra were recorded on a Fisons VG Trio 200 or a Fisons VG Autospec spectrometer. 300 MHz ^{1}H- and ^{13}C-NMR were recorded on a Bruker DPX300 NMR spectrometer. UV/vis spectra were recorded on a Perkin-Elmer Lambda 5 spectrophotometer. IR spectra were recorded on a Nicolet Avatar 360 FTIR spectrometer for samples pressed into a KBr disc.

For all electrochemical experiments, the CH_2Cl_2 was freshly distilled under dinitrogen from calcium hydride. The cyclic voltammogram of each compound (1 mM) in CH_2Cl_2 containing [NBu^n_4][BF_4] (0.4 M) as the background electrolyte was recorded under dinitrogen at room temperature using a glassy carbon working electrode, a Pt wire secondary electrode, and a saturated calomel reference electrode. The cyclic voltammogram of each compound was referenced to the Fc^+/Fc couple that was used as internal standard. When necessary, the [$FeCp_2$*]$^+$/[$FeCp_2$*] couple was used as the internal reference to avoid overlapping redox couples and the potentials of the redox process were referenced to that of Fc^+/Fc ($E_{1/2}$ = 0.540 V *vs.* SCE) couple by an independent calibration. The $\Delta E_{1/2}$ between Fc^+/Fc and [$FeCp_2$*]$^+$/[$FeCp_2$*] recorded under identical conditions was 0.526 V. All potentials were measured *vs.* SCE but are quoted *vs.* Fc^+/Fc. All coulometric measurements were performed at room temperature or 0 °C in a CH_2Cl_2 solution containing [NBu^n_4][BF_4] (0.4 M); the cell consisted of a Pt/Rh gauze basket working electrode, a Pt/Rh gauze secondary electrode, and a saturated calomel reference electrode. Both CV and CPE measurements were made using an Autolab PGSTAT20 potentiostat.

The UV/vis spectroelectrochemical experiments were carried out with an optically transparent thin-layer electrochemical (OTTLE) cell (modified quartz cuvette, optical pathlength: 0.5 mm). A three-electrode configuration, consisting of a Pt/Rh gauze working electrode, a Pt wire secondary electrode (in a fritted PTFE sleeve) and a saturated calomel electrode, chemically isolated from the test solution *via* a bridge tube containing electrolyte solution and terminated in a porous frit, was used in the cell. The potential at the working electrode was controlled by a Sycopel Scientific Ltd. DD10M potentiostat. The UV/vis spectra were recorded on a Perkin-Elmer Lambda 16 spectrophotometer. The spectrometer cavity was purged with dinitrogen and temperature control at the sample was achieved by flowing cooled dinitrogen across the surface of the cell.

X-Ray crystallography

The unit cell, data collection and refinement parameters for LH·Me_2CO, **1**·3MeOH, **2**·2.5MeCN·0.3CH_2Cl_2, and [**2**][BF_4]·

Table 1 Crystallographic data for compounds LH·Me_2CO, **1**·4DMF, **1**·3MeOH, **2**·2.5MeCN·0.3CH_2Cl_2, [**1**][BF_4]·2CH_2Cl_2, and [**2**][BF_4]·2CH_2Cl_2·0.75pentane

	LH·Me_2CO	**1**·4DMF[5]	**1**·3MeOH	**2**·2.5MeCN·0.3CH_2Cl_2	[**1**][BF_4]·2CH_2Cl_2[5]	[**2**][BF_4]·2CH_2Cl_2·0.75pentane
Empirical formula	$C_{32}H_{38}N_2O_2$	$CuC_{70}H_{90}N_8O_6$	$CuC_{61}H_{74}N_4O_5$	$ZnC_{63.3}H_{70.1}N_{6.5}O_2Cl_{0.6}$	$CuC_{60}H_{66}N_8O_2BF_4Cl_4$	$ZnC_{62.5}H_{70.25}N_4O_2BF_4Cl_4$
M	482.64	1203.04	1006.78	1040.60	1167.32	1203.46
Crystal system	Monoclinic	Monoclinic	Triclinic	Monoclinic	Monoclinic	Monoclinic
Space group (no.)	$P2_1/n$ (14)	$C2/c$ (15)	$P\bar{1}$ (2)	$P2_1/n$ (14)	$P2_1/n$ (14)	$P2_1/c$ (14)
a/Å	18.059(2)	29.090(2)	12.207(1)	16.9519(9)	12.6062 (7)	13.964(4)
b/Å	8.5608(9)	13.246(9)	13.790(1)	17.8270(9)	18.2942(10)	17.079(5)
c/Å	19.135(2)	18.630(1)	18.805(2)	19.2760(10)	25.5061(14)	28.310(9)
α/°	90	90	70.972(1)	90	90	90
β/°	106.567(2)	112.506(1)	74.630(2)	102.088(1)	96.191(1)	91.729(6)
γ/°	90	90	68.125(2)	90	90	90
V/Å^3	2835.5(5)	6632.0(7)	2739.5(7)	5696.0(9)	5847.9(9)	6749(3)
Z	4	4	2	4	4	4
T/K	150	150	150	150	150	150
D_c/g cm^{-3}	1.131	1.205	1.220	1.213	1.326	1.18
μ/mm^{-1}	0.070	0.386	0.450	0.510	0.61	0.574
Reflections collected	16919	30269	19728	46084	40636	33249
Independent reflections (R_{int})	6512 (0.064)	8328 (0.035)	12281 (0.043)	13891 (0.078)	14159 (0.043)	15494 (0.054)
Observed reflections [$I > 2\sigma(I)$]	3621	6303	9231	7197	13749	9548
R	0.0481	0.0399	0.0501	0.0525	0.0681	0.1178
R_w	0.1479	0.1124	0.1392	0.1248	0.1888	0.3686

2CH_2Cl_2·0.75pentane are given in Table 1; the details for **1**·4DMF and [**1**][BF_4]·2CH_2Cl_2 are included for comparison.[5] Diffraction data for all of these compounds were collected on a Bruker SMART 1000 CCD area detector diffractometer equipped with an Oxford Cryosystem open-flow nitrogen cryostat[6] using ω-scans and graphite-monochromated Mo-Kα radiation (0.71073 Å). Data were corrected for Lorentz and polarization effects. The structures of LH·Me_2CO and [**2**][BF_4]·2CH_2Cl_2·0.75pentane were solved by direct methods and those of **2**·2.5MeCN·0.3CH_2Cl_2 and **1**·3MeOH by Patterson methods using SHELXS-97.[7a] Each structure was refined against F^2 using SHELXL-97.[7a] Unless otherwise stated, all non-H atoms were refined with anisotropic atomic displacement parameters. The hydrogen atoms of: CH_3CN, CH_3OH, $(CH_3)_2CO$, and PhO*H* were located from difference Fourier syntheses and their positions refined as part of a rigid rotor. All other H-atoms were placed in geometrically calculated positions and refined as part of a riding model, with $U(H)_{iso}$ = $1.2U_{eq}(C)$, for those of C_6H_5 and $U(H)_{iso} = 1.5U_{eq}(C)$, for CH_3. For **2**·2.5MeCN·0.3CH_2Cl_2, a region of the occluded solvent was disordered and modelled as the stated chemical composition with restraints applied to the geometry of the solvent molecules, but their hydrogen atoms were not located. For [**2**][BF_4]·2CH_2Cl_2·0.75pentane, disorder was identified in one CH_2Cl_2 molecule which was modelled over two sites with occupancies of 0.4 : 0.6 and isotropic atomic displacement parameters. Two (partially occupied) pentane molecules were also included in this structure. One site has an occupancy of 0.5; the other molecule is highly disordered and occupies two sites, each of 0.25 occupancy, which overlap (excepting a terminal carbon) and lie across an inversion centre, such that only half of each orientation is in the asymmetric unit. The R-factor of [**2**][BF_4]·2CH_2Cl_2·0.75pentane reflects the generally weak nature of the diffraction data observed at higher scattering angles.

CCDC reference numbers 199488–199491.

See http://www.rsc.org/suppdata/dt/b2/b212209j/ for crystallographic data in CIF or other electronic format.

Results

The pro-ligand LH and the radical cation [LH]$^{\cdot+}$

Synthesis and structure of LH. LH was synthesised by the condensation of 3,5-di-*tert*-butylhydroxybenzaldehyde with benzil (1 : 1) in AcOH in the presence of an excess of [NH_4][OAc] (yield 75%). The structure of LH (in LH·Me_2CO, see Fig. 1, Table 1) involves an essentially co-planar arrangement of the imidazole and phenol rings, the twist angle between these planes being 7.7°; the corresponding angle in the analogous 2-(2′-hydroxyphenyl)imidazole (ImPhOH) is 1.2°.[8] The angles between the mean plane of the imidazole ring and those of the C(6)–C(11) and C(12)–C(17) phenyl rings are 43.4 and 35.8°, respectively. The length of the C–C, C–N, and C–O bonds of the imidazole and phenol groups are as expected (see Fig. 1).[8,9] The N–H group of LH is involved in an intermolecular N–H ··· O hydrogen bond [N(2) ··· O(1S) 2.852(2) Å and N(2)–H(2A) ··· O(1S) 168.8°] to an adjacent acetone molecule. Also, and in respect of the chemical properties of LH, there is a strong intramolecular hydrogen bond (IMHB) between the phenolic O–H group and N(5). The strength of this IMHB, as measured by the O(1) ··· N(5) distance of 2.596(2) Å and the O(1)–H(1) ··· N(5) angle of 150.7°, is very similar to that in ImPhOH[8] [2.545(2) Å and 154(3)°], 2-(pyrazol-1′-yl)- and 2,5-bis(pyrazol-1′-yl)-1,4-dihydroxybenzene [2.558(9) Å, 138(9)° and 2.612(3) Å, 149(4)°, respectively],[10] and 2-(2-hydroxyphenyl)pyrimidine [2.511(3) Å, 153(5)°].[11]

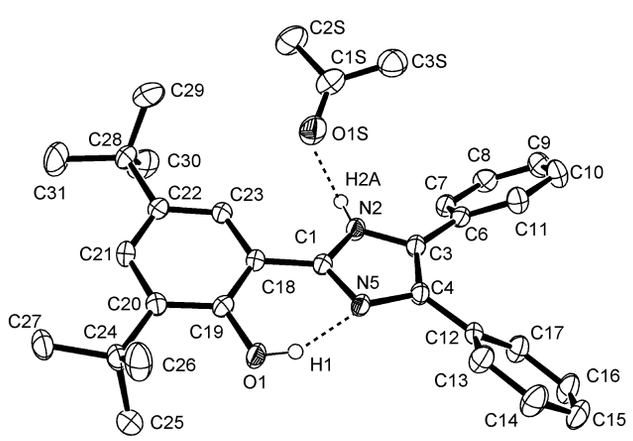

Fig. 1 ORTEP[7b] representation of the structure of LH·Me_2CO. Selected bond lengths: C(19)–O(1) 1.368(2), C(18)–C(19) 1.407(2), C(19)–C(20) 1.402(2), C(20)–C(21) 1.405(2), C(21)–C(22) 1.403(2), C(22)–C(23) 1.384(2), C(23)–C(18) 1.399(2), C(1)–N(5) 1.339(2), C(1)–N(2) 1.360(2) C(3)–N(2) 1.380(2), C(3)–C(4) 1.382(2), C(4)–N(5) 1.385(2), C(1)–C(18) 1.462(2) Å.

Generation and characterisation of $[LH]^{\bullet+}$. The cyclic voltammogram of LH in CH_2Cl_2 at room temperature exhibits a one-electron reversible‡ oxidation at $E_{1/2}$ = 0.43 V *vs.* Fc^+/Fc (E_p^a = 488 mV) (Fig. 2) and an irreversible oxidation at 0.94 V. In contrast, the cyclic voltammogram of *o*,*p*-unprotected analogues of LH,§ recorded under the same conditions, exhibits one irreversible oxidation process at 0. 61 V *vs.* Fc^+/Fc.

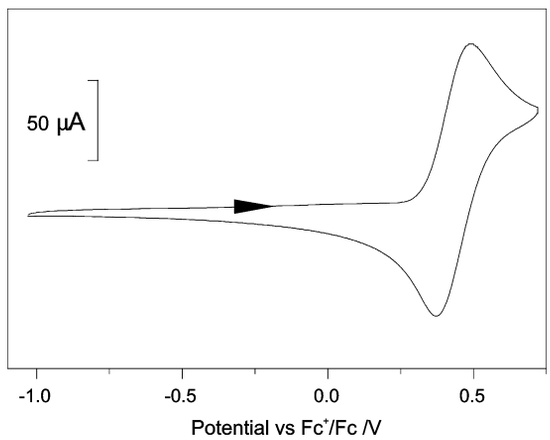

Fig. 2 The cyclic voltammogram of LH (~1 mM) in CH_2Cl_2 at 298 K containing $[NBu_4^n][BF_4]$ (0.4 M) as supporting electrolyte, at a scan rate of 100 mV s^{-1}.

One-electron oxidation of LH, at 0 °C under dinitrogen in CH_2Cl_2 containing 1 mM of LH and $[NBu_4^n][BF_4]$ (0.4 M), by controlled potential electrolysis led to a drastic colour change of the solution from colourless to an intense dark blue. The oxidised species thus produced appeared to remain unchanged for *ca.* 1 h. The X-band EPR spectrum of the oxidised species in CH_2Cl_2 consisted of a single isotropic signal with g_{iso} centered at 2.004 with a line width of ~10 G and no resolved hyperfine splitting.

Electrochemical oxidation of LH, at −40 °C under dinitrogen in CH_2Cl_2 containing 1 mM of LH and $[NBu_4^n][BF_4]$ (0.4 M), was accomplished in an OTTLE cell. A series of smooth changes in the absorbance profile were observed; isosbestic points were observed at 247, 291, and 351 nm and new absorption bands with λ_{max} of 379 (9700), 401 (9200), 514 (4000) and 715 nm (5600 M^{-1} cm^{-1}) (Fig. 3). Electrochemical re-reduction of the oxidised species produced a spectrum corresponding to that originally observed for LH.

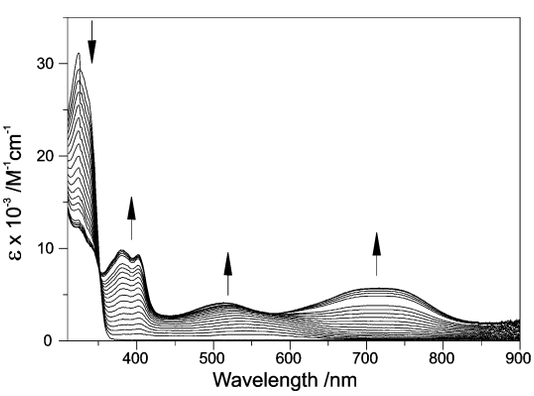

Fig. 3 UV/vis spectra observed during the one-electron oxidation of LH achieved in an OTTLE cell at −40 °C in CH_2Cl_2 containing $[NBu_4^n][BF_4]$ (0.4 M) with an applied potential of 1100 mV *vs.* SCE.

‡ For LH: E_p^a = 488 mV and E_p^c = 379 mV (*vs.* Fc^+/Fc); ΔE = 103–122 mV (scan rate = 20–200 mV s^{-1}); $-i_p^c/i_p^a = 1 \pm 0.1$; (scan rate)$^{1/2} \propto i_p^c$ (and i_p^a). For Fc^+/Fc : ΔE = 73–95 mV (scan rate = 20–200 mV s^{-1}). Controlled potential coulometry of LH at 1.175 V *vs.* SCE indicated the transfer of 1.10 electrons $molecule^{-1}$.

§ The *o*,*p*-unprotected derivative of LH was synthesised using a procedure reported by Mahesh *et al.*[38]

$[CuL_2]$ (1) and $[ZnL_2]$ (2)

Synthesis and structural characterisation. The reaction of $M(BF_4)_2 \cdot H_2O$ (M = Cu, Zn) with LH (1 : 2) in the presence of an excess of Et_3N, yielded the corresponding $[ML_2]$ compound (**1** M = Cu; **2** M = Zn). The crystal structures of **1**·3MeOH, **1**·4DMF and **2**·2.5MeCN·0.3CH_2Cl_2 have been determined by X-ray crystallography (Table 1). In each case, the metal centre possesses an N_2O_2-coordination sphere with each ligand acting as an *N*,*O*-bidentate chelate (Fig. 4a–c). The average length of the M–O and M–N bonds (Table 2) are similar to those of bis(salicylaldiminato)M(II) complexes of the corresponding metal,[12] consistent with the formulation of each compound as an M(II) centre ligated by two monoanionic phenolate *N*,*O*-donor ligands, L^-. Each compound incorporates some solvent molecules in the lattice, some of which engage in hydrogen bonds with the N–H/imidazole and/or O/phenolate groups. Thus, for Me*C*N, Me*O*H, or DMF(*O*), the atom possessing a lone pair of electrons is hydrogen bonded to the imidazole N–H group and MeO*H* forms a hydrogen bond with the phenolate oxygen (Fig. 4a–c).

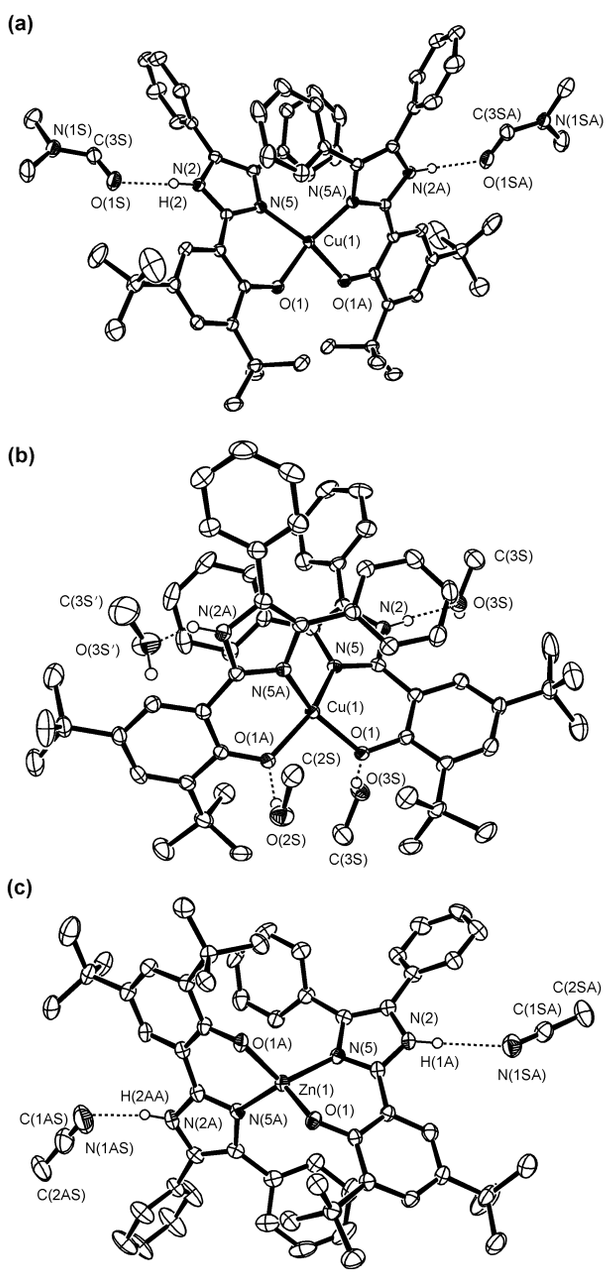

Fig. 4 ORTEP[7b] representation of: (a) **1**·4DMF; (b) **1**·3MeOH and (c) **2**·2.5MeCN·0.3CH_2Cl_2. Only the solvent molecules that are involved in hydrogen bonding interactions with the complex are shown.

Table 2 Selected bond lengths (Å) and angles (°) for **1**·4DMF and **1**·3MeOH (M = Cu) and **2**·2.5MeCN·0.3CH_2Cl_2 (M = Zn)

	1·4DMF	**1**·3MeOH	**2**·2.5MeCN·0.3CH_2Cl_2
M(1)–O(1)	1.899(1)	1.919(2)	1.914(2)
M(1)–O(1A)	1.899(1)	1.913(2)	1.907(2)
M(1)–N(5)	1.958(1)	1.952(2)	1.996(2)
M(1)–N(5A)	1.958(1)	1.945(2)	1.993(2)
O(1A)–M(1)–O(1)	86.23(6)	95.33(6)	111.21(8)
N(5A)–M(1)–N(5)	101.27(7)	100.58(7)	123.02(9)
O(1A)–M(1)–N(5)	154.22(5)	148.97(7)	115.57(8)
O(1)–M(1)–N(5A)	154.22(5)	149.28(7)	118.07(8)
O(1A)–M(1)–N(5A)	91.46(5)	90.15(7)	95.52(8)
O(1)–M(1)–N(5)	91.46(5)	90.10(7)	94.53(8)

The Cu(II) centre of **1**·4DMF possesses a distorted square planar coordination geometry; the angle between the Cu(1)-N(5)O(1) and Cu(1)N(5A)O(1A) planes is 34.5°, whereas the corresponding angle for **1**·3MeOH is 44.0°, *i.e.* closer to that of a distorted tetrahedron. Moreover, there are some significant differences in the length of chemically equivalent Cu–O bonds that appear to be associated with the presence of intermolecular solvent/complex hydrogen bonding. Thus, in **1**·3MeOH, in which each co-ordinated phenolate oxygen is hydrogen bonded to a MeOH molecule, each Cu–O bond [Cu(1)–O(1) = 1.919(2) and Cu(1)–O(1A) = 1.913(2) Å] is significantly longer than the Cu–O bonds in **1**·4DMF [Cu(1)–O(1) = Cu(1)–O(1A) = 1.899(1) Å], for which there is no corresponding interaction.

The Cu(II) centres of **1**·4DMF and **1**·3MeOH each possesses a *cis*-CuN_2O_2 geometry. One side of each of the complexes is occupied by two *o*,*p*-substituted phenolate groups whilst the other side is occupied by the two bulky 4,5-disubstituted imidazole groups.

The Zn(II) centre of **2**·2.5MeCN·0.3CH_2Cl_2 possesses a distorted tetrahedral coordination geometry; the angle between the Zn(1)O(1)N(5) and Zn(1)O(1A)N(5A) planes is 90.3° and the four N–Zn(1)–O interligand angles range from 111 to 118° (Table 2). The lengths of the Zn–O and Zn–N bonds are in good agreement with those found for bis-salicyldiminato-Zn(II)[13] complexes and other Zn(II) complexes containing two phenolate *O*-donor and two *N*-donor ligands.[14]

EPR and UV/vis spectra. The X-band and K-band EPR spectra of **1** in frozen CH_2Cl_2–toluene (9 : 1) solution are shown in Fig. 5. The EPR spectra are typical of a Cu(II) complex possessing a $(d_{x^2-y^2})^1$ or $(d_{xy})^1$ ground state (S = 1/2), with $g_{zz} > g_{xx} \approx g_{yy}$.[15] The X-band EPR spectrum of **1** displays hyperfine and superhyperfine features in the g_{xx}/g_{yy} region, resulting from the interaction of the unpaired electron with the nuclear spin of ^{63,65}Cu (I = 3/2) and with the nuclear spin of the coordinated nitrogen atoms (^{14}N; I = 1); ^{14}N superhyperfine coupling is also apparent in the g_{zz} region of the X-band spectrum (Fig. 5a, inset). Spin-Hamiltonian parameters for **1** have been extracted by the simultaneous simulation of the X- and K-band EPR spectra of **1** using an in-house program.[16] The best fit yielded: g_{xx} = 2.053, g_{yy} = 2.047, g_{zz} = 2.253; $A_{zz}\{^{63,65}\text{Cu}\}$ = 164 G, $A_{xx}\{^{63,65}\text{Cu}\} = A_{yy}\{^{63,65}\text{Cu}\}$ = 29 G, and $a_{xx} = a_{yy} = a_{zz} = a\{^{14}\text{N}\}$ = 12 G. The A_{zz} and g_{zz} values observed are typical of those of a tetragonal Cu^{II}–N_2O_2 centre[17] and indicate that the N_2O_2-coordination sphere of **1** is retained in solution. As expected, **2** is EPR-silent.

The UV/vis absorption spectrum of **1** in CH_2Cl_2 at room temperature is characterised by two bands in the visible region at 499 (670) and 692 nm (550 M^{-1} cm^{-1}). The former absorption resembles that of other Cu(II)-phenolate systems (λ_{max} 450–530 nm; ε 1000–2000 M^{-1} cm^{-1})[18] which have been assigned to a phenolate-to-Cu(II) charge transfer transition (LMCT). This assignment is extended to include the 499 nm band of **1**. The band at 692 nm is assigned to a ligand field (d ⟶ d) transition on the basis of comparisons with distorted square planar bis-(salicylaldiminato)Cu(II) complexes that typically contain an absorption at similar wavelength.[19] **2** does not manifest any absorptions in the visible region.

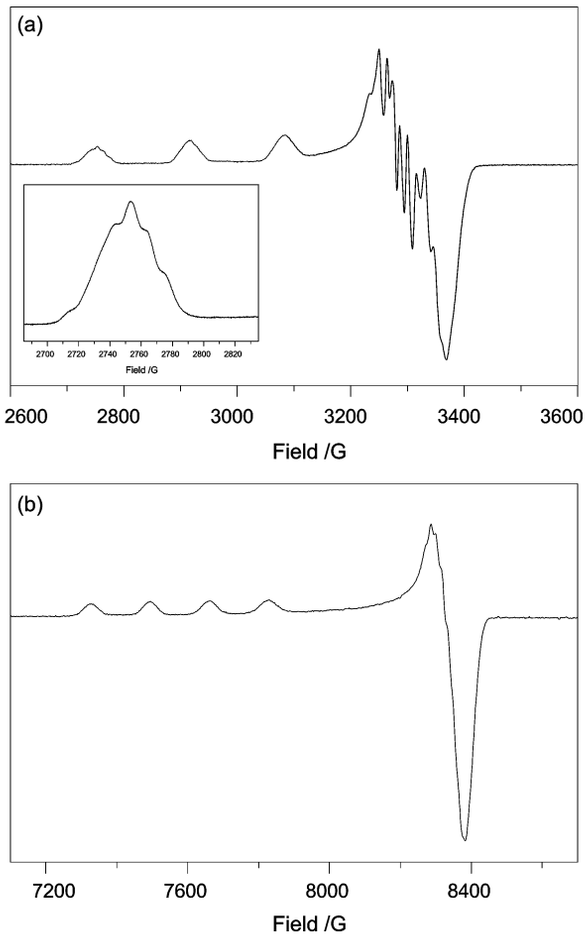

Fig. 5 EPR spectra of **1**: (a) X-band spectrum of a solution of **1** in CH_2Cl_2–toluene (9 : 1) at 77 K; (inset) zoom of one of the peaks in the g_{zz} region showing superhyperfine structure; (b) K-band spectrum of a solution of **1** in CH_2Cl_2–toluene (9 : 1) at 125 K.

Redox properties of 1 and 2. The cyclic voltammogram of **1** (Fig. 6a) in CH_2Cl_2 at room temperature displays two, reversible, one-electron oxidation processes at 0.16 and 0.50 V *vs.* Fc^+/Fc (Table 3) and an irreversible reduction process in the region −1.5 to −1.8 V *vs.* Fc^+/Fc with no apparent associated oxidation. Similarly, the cyclic voltammogram of **2** (Fig. 6b), in CH_2Cl_2 at room temperature exhibits a reversible one-electron oxidation at 0.23 V *vs.* Fc^+/Fc and an essentially reversible couple at 0.49 V *vs.* Fc^+/Fc (Table 3).¶ However, no cathodic peak was observed in the region 0 to −2.5 V *vs.* Fc^+/Fc.

In addition to these electrochemical processes, both **1** and **2** exhibit further oxidation process(es) at 0.962 and 1.130 (**1**); and 1.034 (**2**) V *vs.* Fc^+/Fc, each of which is irreversible.

The close correspondence between the electrochemical properties of **1** and **2** indicates that the two reversible oxidation

¶ For the redox process at 0.49 V (*vs.* Fc^+/Fc) of **2**, $-i_p^c/i_p^a = 1 \pm 0.1$, $(\text{scan rate})^{1/2} \propto i_p^c$ (and i_p^a) and ΔE = 148 mV. A slight shoulder was observed on the second oxidation wave for both **1** and **2** (Fig. 6). The controlled potential electrolysis of **1** at 0.78 (at rt) and 1.25 V (at 0 °C) (*vs.* SCE) indicated the transfer of 0.91 and 1.86 electrons $molecule^{-1}$, respectively. The controlled potential electrolysis of **2** at 0.87 (at rt) and 1.20 V (at 0 °C) (*vs.* SCE) indicated the transfer of 1.00 and 2.14 electrons $molecule^{-1}$, respectively.

Table 3 Cyclic voltammetric data for **1** and **2** recorded in CH_2Cl_2 at 298 K. The potentials are expressed in V *vs.* $[Fc]^+/[Fc]^a$

	Cu^{II}/Cu^{I}	First ligand-based process		Second ligand-based process	
	E_p^c	E_p^a (ΔE/mV)	$E_{1/2}$	E_p^a (ΔE/mV)	$E_{1/2}$
1	−1.5 to −1.8	0.202(87)	0.16	0.540(90)	0.50
2	—	0.269(87)	0.23	0.567(148)	0.49

ΔE = 106 mV for $[FeCp^*]^+/[FeCp^*]$.[a] These data have been redetermined; as compared to the data reported previously,[5] the $E_{1/2}$ values differ by ≤0.02 V.

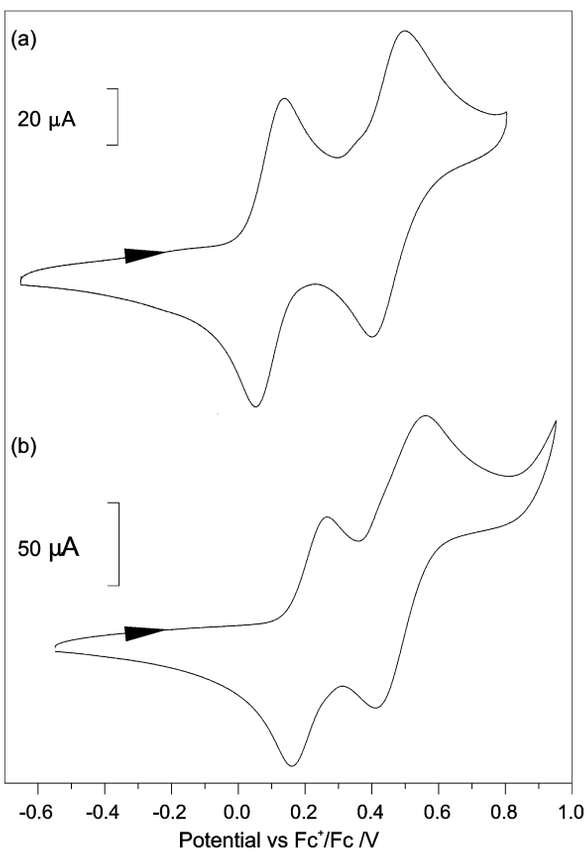

Fig. 6 Cyclic voltammogram of (a) **1** and (b) **2**, recorded for a CH_2Cl_2 solution at 298 K containing $[NBu_4^n][BF_4]$ (0.4 M) as the supporting electrolyte, using a glassy carbon working electrode at a scan rate of 100 mV s^{-1}.

processes observed (Fig. 6) are ligand-based, especially since Zn(II) is not redox active. Thus, these processes are attributed to the successive one-electron oxidation of each coordinated ligand, leading to the formation of $[M(L^{\bullet})(L)]^+$ initially and then $[M(L^{\bullet})]^{2+}$, these complexes involve one or two neutral radical ligands, $L^{\bullet}$; respectively (Scheme 1). The reversibility observed for both oxidation processes indicates that $[M(L^{\bullet})(L)]^+$ and $[M(L^{\bullet})_2]^{2+}$ do *not* decompose during the course of the cyclic voltammetric experiment. The irreversible reduction processes observed in the region −1.5 to −1.8 V *vs.* Fc^+/Fc for **1**, but not for **2**, is attributed to the Cu(II)/Cu(I) couple.

$$[ML_2] \underset{+1e^-}{\overset{-1e^-}{\rightleftharpoons}} [M(L^{\bullet})(L)]^+ \underset{+1e^-}{\overset{-1e^-}{\rightleftharpoons}} [M(L^{\bullet})_2]^{2+}$$

Scheme 1

The phenoxyl radical complexes $[M(L^{\bullet})(L)]^+$

Electrochemically generated $[1]^+$ and $[2]^+$. Electrochemical one-electron oxidation of **1** and **2**, at room temperature in CH_2Cl_2 solution containing $[NBu_4^n][BF_4]$ (0.4 M) under a dinitrogen atmosphere, with an applied potential of 0.78 and 0.87 V *vs.* SCE, respectively, induced a drastic colour change. Thus, in each case an intense, dark green coloured solution was produced, due to the formation of the oxidation product $[\mathbf{1}]^+$ and $[\mathbf{2}]^+$, respectively. Remarkably, these oxidised species were found to be stable under these conditions.

In contrast to the EPR spectrum of **1** which exhibits an $S = ½$ signal, typical of Cu(II) in an axial ligand field, $[\mathbf{1}]^+$ in CH_2Cl_2 (containing $[NBu_4^n][BF_4]$ (0.4 M)) at 77 K, was found to be EPR-silent [NB a weak (<10% of the intensity observed for **1**) Cu(II) signal was observed]. The lack of an EPR signal for $[\mathbf{1}]^+$ is consistent with a $S = 0$ or 1 ground state, resulting from the magnetic coupling between the $S = ½$ Cu(II) centre and a $S = ½$ co-ordinated radical ligand, as has been observed for other Cu(II)-phenoxyl radical complexes.[18]

The EPR spectrum of $[\mathbf{2}]^+$, in CH_2Cl_2 at 77 K, consists of a single isotropic signal with g_{iso} = 2.0047. This EPR spectrum does not exhibit any hyperfine splitting and possesses a line width of ~10 G. The $S = ½$ EPR signal obtained for $[\mathbf{2}]^+$ is typical of that for a radical and the *g*-value is within the range of those reported for Zn(II)-phenoxyl radical compounds.[20]

The OTTLE spectra recorded for the one-electron oxidation of **1** and **2**, in CH_2Cl_2, containing $[NBu_4^n][BF_4]$ (0.4 M) at 0 °C, each shows a series of changes in the absorbance profile (Fig. 7). The observation of isosbestic points indicate that the oxidation of **1** and **2**, produces a single species, $[\mathbf{1}]^+$ or $[\mathbf{2}]^+$, directly and without the involvement of any detectable intermediate. In each case, the electrochemical reduction of $[\mathbf{1}]^+$ and $[\mathbf{2}]^+$ returned the UV/vis spectrum to the profile of the corresponding ML_2 compound, confirming the chemical reversibility of the one-

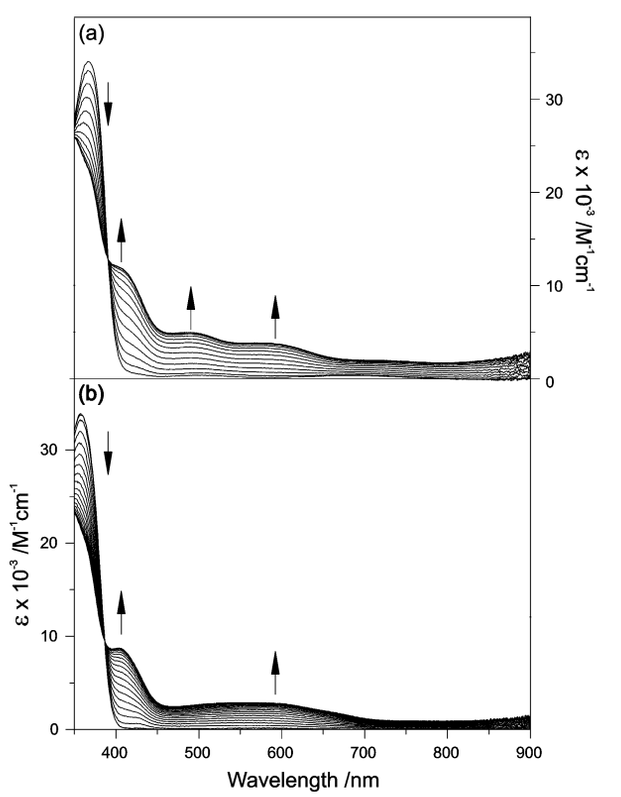

Fig. 7 UV/vis spectra recorded for the one-electron oxidation of **1** and **2** in an OTTLE cell with an applied potential of 865 and 845 mV *vs.* SCE, respectively. Each experiment was carried out at 0 °C for a solution of **1** and **2** (~1 mM) in CH_2Cl_2 containing $[NBu_4^n][BF_4]$ (0.4 M) as the supporting electrolyte. λ_{max}/nm (ε/M^{-1} cm^{-1}) for $[\mathbf{1}]^+$: 278 (40900), sh 299(38000), br 346 (25900), sh 368 (22200), sh 408 (11800), 484 (4900), 580 (3800), 670–900 (1700); λ_{max}/nm (ε/M^{-1} cm^{-1}) for $[\mathbf{2}]^+$: 225 (63000), br 279 (37240), br 356 (22000), sh 410 (8500), br *ca.* 560 (2870), 700–850 (1000). Isosbestic points for the oxidation of **1**: 262, 291, 351, 391 nm and for **2**: 262, 334, 385 nm.

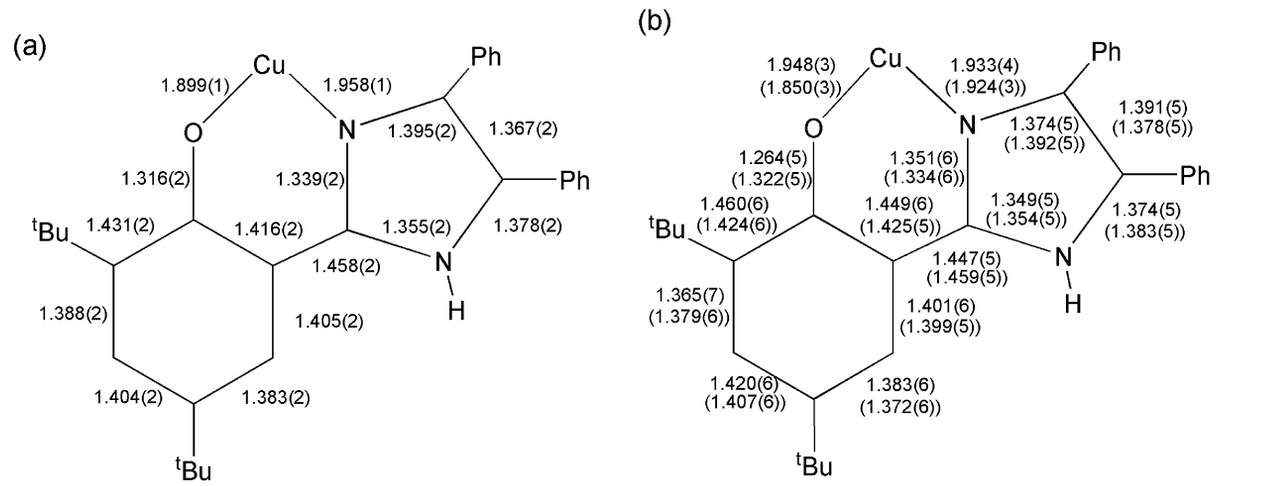

Fig. 8 Selected bond lengths (Å) of (a) **1**·4DMF, in which the two ligands are related by a C_2 axis and (b) the cation of [**1**][BF_4]·2CH_2Cl_2 containing L^A and L^B (values for the latter are given in parentheses).

electron electrochemical process on the time scale of the OTTLE experiment.

The absorption spectrum of [**1**]$^+$ and [**2**]$^+$ each exhibits an intense absorption at *ca.* 410 nm (ε/M^{-1} cm^{-1}: 11800 [**1**]$^+$; 8500 [**2**]$^+$) and less intense broad absorptions between 500 and 900 nm (Fig. 7). The absorption at *ca.* 410 nm is assigned to the $\pi \longrightarrow \pi^*$ transition of the phenoxyl radical ligand, as observed in the UV/vis spectra of several other Cu(II)- and Zn(II)-phenoxyl radical complexes.[18,20] The lower energy band could arise from ligand-based transitions ($\pi \longrightarrow \pi^*$ or $n \longrightarrow \pi^*$), MLCT, LMCT, and/or LLCT transitions. Since these absorptions occur for both [**1**]$^+$ and [**2**]$^+$, they can not arise from $d \longrightarrow d$ transitions.

Chemically generated [1]$^+$ and [2]$^+$. The one-electron oxidation of **1** and **2** by Ag[BF_4] (1 eq.) in CH_2Cl_2 produced the dark green compounds [**1**][BF_4] and [**2**][BF_4], respectively. These compounds were found to be inert in the solid state, even when exposed to air, and a solution of each of these compounds in CH_2Cl_2, at room temperature under an argon atmosphere, remained unchanged for several days. The remarkable inertness of these compounds has permitted their structural, spectroscopic, and magnetic characterisation.

Spectroscopic and electrochemical investigations. The UV/vis spectra of [**1**][BF_4] and [**2**][BF_4], in CH_2Cl_2 at 0 °C, were essentially identical to those of the corresponding species generated electrochemically. The room temperature X-band EPR spectrum of [**1**][BF_4], in the solid and CH_2Cl_2 solution states, was found to be EPR-silent over the magnetic field range of 0–6000 G. The 77 K X-band EPR-spectrum of [**1**][BF_4] in CH_2Cl_2 solution showed a weak signal which was attributed to the presence of ~5% of unreacted starting material **1**.

The X-band EPR spectrum of [**2**][BF_4] at 77 K in CH_2Cl_2 solution exhibited a signal at g_{iso} = 2.0047 with a line width of ~10 G and no observable hyperfine splitting. This signal is essentially identical to that obtained for the corresponding electrochemically generated species (g_{iso} = 2.004).

The cyclic voltammograms of [**1**][BF_4] and [**2**][BF_4], in CH_2Cl_2 at room temperature, were identical to that of the corresponding parent compound.

Thus, each of the cations [**1**]$^+$ (in [**1**][BF_4]) and [**2**]$^+$ (in [**2**][BF_4]) is identical to the corresponding electrochemically generated species.

Structural investigations

[1][BF_4]·2CH_2Cl_2. The X-ray crystallographic characterisation of [**1**][BF_4]·2CH_2Cl_2 (see Figs. 8 and 9 and Table 1) confirms the formation of [**1**]$^+$ as the product of the chemical

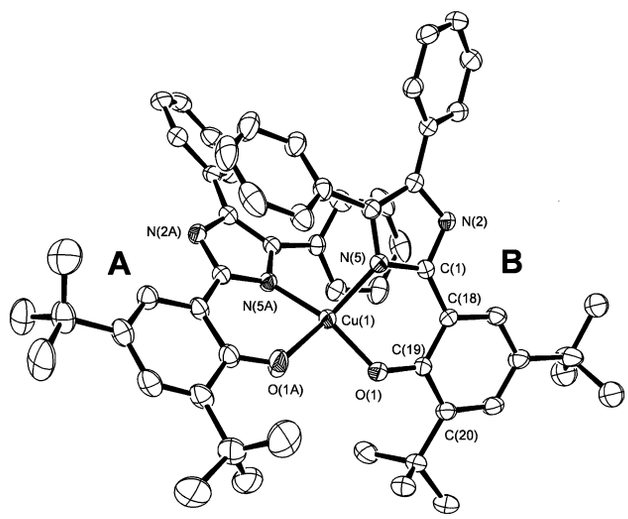

Fig. 9 An ORTEP[7b] representation of the structure of [**1**]$^+$ in [**1**][BF_4]·2CH_2Cl_2.

one-electron oxidation of **1**. The copper centre of [**1**][BF_4] possesses a *cis*-arrangement of the phenol *O*-donor atoms; *i.e.* the two 4,5-diphenyl imidazole units are accommodated on the same side of the complex, as in **1**.

In comparing the dimensions of [**1**]$^+$ with the corresponding values of **1**, attention is confined to **1**·4DMF since, in **1**·3MeOH, possible perturbations arise due to the presence of MeO–H ··· O(phenolate) hydrogen bonds. The structural details of [**1**]$^+$ differ slightly, but significantly, from the corresponding aspects of **1** in **1**·4DMF (Fig. 8). The dihedral angle between the two Cu(1)O(1)N(5) and Cu(1)O(1A)N(5A) intraligand planes is 46.9° which is larger than the corresponding angles in **1**·4DMF and **1**·3MeOH (34.5 and 44.0°, respectively).

The two ligands of **1**·4DMF are related by a C_2-axis, but the two ligands of [**1**]$^+$ in [**1**][BF_4]·2CH_2Cl_2, designated as L^A and L^B (Figs. 8 and 9), are inequivalent. For L^B, the length of each C–C, C–O, and C–N bond is not significantly different from the length of the corresponding bonds in **1**·4DMF. However, for L^A, the C–O distance [1.264(5) Å] is significantly *shorter* than that in **1** [1.316(2) Å] and that in L^B [1.322(5) Å]. Also, the two C–C bonds adjacent to the C–O group of L^A [C(18A)–C(19A) = 1.449(6) Å and C(19A)–C(20A) = 1.460(6) Å] are each significantly *longer* than the corresponding bonds of both **1** [1.416(2) and 1.431(2) Å, respectively] and L^B [1.425(5) and 1.424(6) Å, respectively]. Furthermore, the length of the Cu–O bond involving L^A [1.948(3) Å] is significantly *longer* than that in **1**·4DMF [1.899(1) Å], but the length of each of the other three

metal–ligand bonds in $[\mathbf{1}]^+$ [Cu–O(1) = 1.850(3) Å, Cu–N(5) = 1.924(3) Å and Cu–N(5A) = 1.933(4) Å] is each significantly *shorter* than that of its counterpart in **1**·4DMF [Cu–O = 1.899(1) Å and Cu–N = 1.958(1) Å] (Fig. 8).

This structural information is taken to indicate that $[\mathbf{1}]^+$ contains both a phenoxyl radical ($L^A = L^\bullet$) and a phenolate ($L^B = L^-$) ligand coordinated to Cu^{II}; *i.e.* $[\mathbf{1}]^+$ is constituted as $[Cu^{II}(L^\bullet)(L^-)]^+$. Oxidation of a phenolate ligand in **1** to a phenoxyl radical in $[\mathbf{1}]^+$ is accompanied by a shortening of the C–O bond and the lengthening of the two adjacent C–C bonds. The changes in the length of these C–O and C–C bonds are in accord with a description of the electronic structure of $L^\bullet$ by the two resonance forms shown in Fig. 10, *i.e.* the unpaired electron is delocalised over both *ortho* positions of the coordinated phenoxyl ring. The shorter C–O bond length in $L^\bullet$, as compared to that in L^-, is consistent with the structural information that has been obtained for $[Cr^{III}L]^+$ [H_3L = 1,4,7-tris(3-*tert*-butyl-5-methoxy-2-hydroxybenzyl)-1,4,7-triazacyclononane] with one phenoxyl radical and two phenolate ligands. In $[Cr^{III}L]^+$ the length of the C–O bond of the phenoxyl radical [1.290(4) Å] is significantly less than that of the two phenolate ligands [1.328(6) and 1.342(4) Å].[21] In $[\mathbf{1}]^+$ the length of the C–O bond of L^A of 1.264(5) Å emphasising a significant amount of double bond character (see Fig. 8) in this bond. As compared to **1**·4DMF, the shortening of the C–O bond in L^A is accompanied by a lengthening of the corresponding Cu–O bond and the contraction of the three other Cu–O/N bonds, consistent with the oxygen atom of the phenoxyl ($L^\bullet$) donating relatively less electron density to the Cu(II) than the oxygen of the phenoxide (L^-).

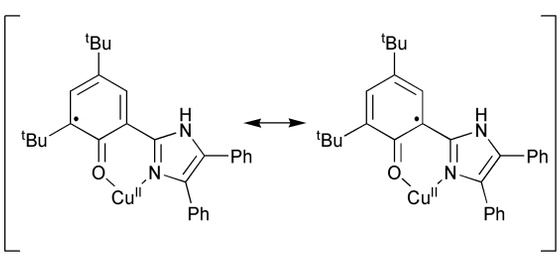

Fig. 10 Resonance forms of $L^\bullet$ in $[Cu^{2+}(L^\bullet)(L^-)][BF_4]$.

$[2][BF_4]\cdot 2CH_2Cl_2\cdot 0.75$pentane. Although single crystals of $[\mathbf{2}][BF_4]\cdot 2CH_2Cl_2\cdot 0.75$pentane of a reasonable quality and size were obtained, the structure of this compound could be only partially determined by X-ray crystallography. This situation prevailed despite repeated attempts to collect good quality diffraction data by employing longer scan times, larger crystals, and a lower sample temperature (85 K). The problems encountered may arise due to disordered solvent molecules within the lattice of the crystal. Nevertheless, the structural information clearly indicates a stoichiometry of $[\mathbf{2}][BF_4]$, consistent with the presence of $[\mathbf{2}]^+$ (Fig. 11 and Table 1). The zinc is bound to two *N*,*O*-bidentate ligands, L^A and L^B, (Fig. 11) and the complex has a tetrahedral N_2O_2-coordination sphere; the dihedral angle between the two Zn(1)O(1)N(5) and Zn(1)O(1A)N(5A) intraligand planes is 95.5°, similar to that (90.3°) of **2**. A comparison of the dimensions of $[\mathbf{2}]^+$ and **2** shows some important structural changes about the Zn(II) (Table 4). Zn–O(1A) in $[\mathbf{2}]^+$ is significantly *longer* than both Zn–O bonds in **2**, however, each of the other three Zn–O/N bonds in $[\mathbf{2}]^+$ is significantly shorter than that of the corresponding bonds in **2** (Table 4). This pattern resembles that of $[\mathbf{1}]^+$ and is consistent with the formulation of $[\mathbf{2}]^+$ as $[Zn^{II}(L^\bullet)(L^-)]^+$, with L^A being $L^\bullet$. However, the large uncertainties in the C–C, C–N and C–O bond lengths of $[\mathbf{2}]^+$ preclude any assessments of the changes in the dimensions within each coordinated ligand.

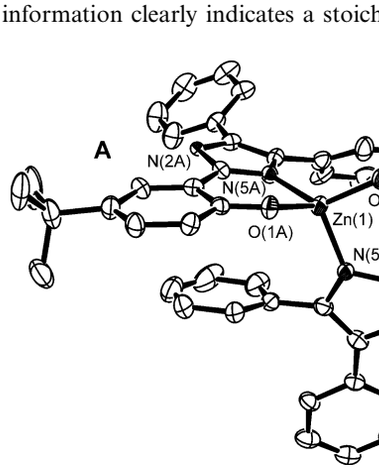

Fig. 11 An ORTEP representation of the structure of $[\mathbf{2}][BF_4]$ in $[\mathbf{2}][BF_4]\cdot 2CH_2Cl_2\cdot 0.75$pentane.

Table 4 Selected bond lengths (Å) for the Zn centre in $[\mathbf{2}]\cdot 2.5MeCN\cdot 0.3CH_2Cl_2$ and $[\mathbf{2}][BF_4]\cdot 2CH_2Cl_2\cdot 0.75$pentane

	$[\mathbf{2}][BF_4]\cdot 2CH_2Cl_2\cdot$ 0.75pentane	$[\mathbf{2}]\cdot 2.5MeCN\cdot$ $0.3CH_2Cl_2$
Zn–O(1)	1.875(5)	1.914(2)
Zn–O(1A)	1.997(6)	1.907(2)
Zn–N(5)	1.950(6)	1.996(2)
Zn–N(5A)	1.976(5)	1.993(2)

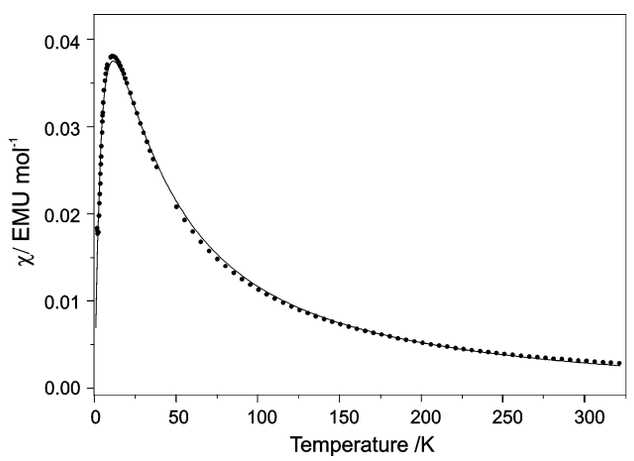

Fig. 12 Variation of χ *vs.* T for $[\mathbf{1}][BF_4]$; the solid line represents a simulation of the experimental data.

Magnetic properties of $[\mathbf{1}][BF_4]$. The temperature dependence of the magnetic susceptibility of $[\mathbf{1}][BF_4]$ over the temperature range 3 to 320 K (Fig. 12) exhibits a maximum (at *ca.* 12 K) indicative of an antiferromagnetic interaction. The variation of χ with T (Fig. 12) has been modelled successfully by the Hamiltonian $H = -2JS_{Cu}S_{rad}$ ($J = -6.1$ cm^{-1}; $S_{Cu} = S_{rad} = ½$; $g_{Cu} = 2.12$; $g_{rad} = 2.00$).[5] Thus, $[\mathbf{1}][BF_4]$ possesses a diamagnetic ground state ($S = 0$) that is considered to arise from an antiferromagnetic coupling between the unpaired electron of the Cu(II) and the unpaired electron of the coordinated phenoxyl radical, $L^\bullet$.[5]

Discussion

This study has accomplished the design, synthesis, and characterisation of the pro-ligand LH and shown that this molecule is capable of undergoing a reversible, one-electron, oxidation to form the radical cation $[LH]^{\bullet+}$. $[LH]^{\bullet+}$ has been produced by electrochemical oxidation. The spectroscopic characteristics observed are consistent with $[LH]^{\bullet+}$ being a phenoxyl radical cation; *i.e.* the unpaired electron is delocalised, primarily or exclusively, over the phenol group. Thus, this moiety exhibits intense absorptions in the visible region, in particular two bands at *ca.* 400 nm (ε *ca.* 10000 M^{-1} cm^{-1}), that resemble the absorptions observed for phenoxyl radicals[22a] and phenoxyl

radical cations.[22–24] Also, the EPR spectrum of $[LH]^{\bullet+}$ comprises a signal with a *g*-value (2.004) that is typical of an organic radical. The lack of any hyperfine structure in the EPR spectrum of $[LH]^{\bullet+}$ precludes any analysis of the spin density distribution within this species. However, since the line width of the signal is relatively narrow (*ca*. 10 G), any hyperfine splitting will be relatively small; this may indicate that the unpaired electron is not (or only to a limited extent) localised on the *N*-imidazole atoms.

The reversible cyclic voltammogram of LH is remarkable and unexpected for a phenol-containing compound. Indeed, the cyclic voltammograms of phenols that are capable of forming a stable phenoxyl radical (*e.g.* 2,4,6-tri-*tert*-butylphenol)[22a] exhibit, in non-basic media, a *two*-electron irreversible oxidation.[25] One-electron oxidation produces the phenoxyl radical cation, $[PhOH]^{\bullet+}$, that contains a strongly acidic $^{\bullet}$O–H group (pK_a *ca.* −5)[22b] that is readily deprotonated to form the phenoxyl radical, $[PhO]^{\bullet}$. The latter is more easily oxidised than the corresponding PhOH (*e.g.* in MeCN, the 2,4,6-tri-*tert*-butylphenoxyl radical is oxidised at a potential *ca.* 300 mV less than that required to oxidise the phenol)[26] and, consequently, undergoes a further one-electron oxidation to form the $[PhO]^{+}$ cation.[25]

The crystal structure of LH clearly shows the presence of a strong O–H ··· N intramolecular hydrogen bond between the phenol and imidazole groups (Fig. 1). The reversibility of the electrochemical oxidation of LH indicates that $[LH]^{\bullet+}$ retains this phenolic proton, presumably now involved in an $^{\bullet}$O–H ··· N intramolecular hydrogen bond (Fig. 13). The results of other investigations support this postulate. Firstly, apart from the results reported herein, only three phenolic compounds have been reported to exhibit an oxidation that is electrochemically reversible; in each case, the electrochemistry was accomplished in an acidic medium.[27] Secondly, Maki *et al.*[23] reported the first example of reversible electron transfer between a phenol and its phenoxyl radical cation and showed that this was facilitated by intramolecular hydrogen bonding. This study involved a 2,4-di-*tert*-butylphenol that was substituted at the 6-position by an α-alkylamino group, thus allowing the formation of a six-membered ring involving an O–H ··· N intramolecular hydrogen bond (*cf*. that for LH, Fig. 1). The EPR (g_{iso} = 2.0046; line width 10 G, no hyperfine splitting) and UV/vis (λ_{max} 386 and 404 nm) properties of this phenoxyl radical cation are very similar to those of $[LH]^{\bullet+}$. Therefore, it appears that the presence of an $^{\bullet}$O–H ··· N intramolecular hydrogen bond, between the phenoxyl radical and the *N*-imidazole group, makes a significant contribution to the stability of $[LH]^{\bullet+}$. Such an interaction is strikingly similar to that proposed between the Tyr160 (Y_D) radical and the adjacent His189 residue in PSII.[28]

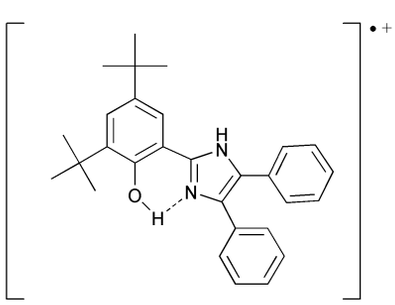

Fig. 13 The intramolecular hydrogen bonding in $[LH]^{\bullet+}$.

The structural details obtained for **1** and **2** have shown that normal geometrical preferences of these M(II) centres are adopted; *i.e.* the CuN_2O_2 core of **1** is distorted square planar and the ZnN_2O_2 core of **2** is essentially tetrahedral. The small angular and radial variations observed between the Cu(II) centres of **1**·4DMF and **1**·3MeOH are presumably due to different metal complex/solvent interactions, indicating that small distortions of this CuN_2O_2 coordination sphere can be achieved relatively easily.

1 adopts a *cis*-arrangement, *i.e.* the O(1)Cu(1)O(1A) and N(5)Cu(1)N(5A) angles (*ca.* 90° and *ca*. 100°, respectively) are smaller than the O(1)Cu(1)N(5A) and O(1A)Cu(1)N(5) angles (*ca.* 150°), indicating the relative proximity of O(1) to O(1A) and of N(5) to N(5A). A *cis*-arrangement is rarely encountered for a Cu(II) centre bound to two *N*,*O*-bidentate ligands that involve phenolate groups, *e.g.* no such example has been reported for a bis-salicylaldiminato-Cu(II) complex. Also, the adoption of the *cis*-geometry is surprising since the 4,5-diarylimidazole groups are sterically demanding.[29] However, the adoption of this arrangement may be rationalised by considering interligand π–π interactions (*vide infra*).

The one-electron oxidation of **1** and **2** forms $[\mathbf{1}]^{+}$ and $[\mathbf{2}]^{+}$, respectively. These cations are remarkably stable, both in solution and the solid state, at or below room temperature. The nature of $[\mathbf{1}]^{+}$ and $[\mathbf{2}]^{+}$ has been confirmed by the X-ray crystallographic investigations of $[\mathbf{1}][BF_4]\cdot 2CH_2Cl_2$ and $[\mathbf{2}][BF_4]\cdot 2CH_2Cl_2\cdot 0.75$pentane. These studies have shown that the geometry around the metal centre of each $[ML_2]^{+}$ cation is very similar to its $[ML_2]$ counterpart. However, there are small, but significant variations in the length of the M–O/N bonds and, for **1** *vs*. $[\mathbf{1}]^{+}$, in the lengths of the C–O and the adjacent C–C bonds. These variations are consistent with the formulation of these cations as $[M^{II}(L^{\bullet})(L^{-})]^{+}$ (M = Cu, Zn), containing a phenoxyl radical and a phenoxide ligand. In respect of this information, it is interesting to note that Cu K-edge X-absorption spectroscopic studies have indicated that there are no major structural differences in the Cu(II) coordination spheres of the inactive and the active (Cu(II)-tyrosinyl) forms of GAO.[30]

The UV/vis and EPR properties of $[\mathbf{1}]^{+}$ and $[\mathbf{2}]^{+}$ are also consistent with each of these species being constituted as a $[M(L^{\bullet})(L)]^{+}$ complex. The potential for the first oxidation of **1** and **2** is less positive than that for the oxidation of LH, by 286 and 219 mV, respectively; *i.e.* compared to the phenol, the binding of a phenolate to Cu(II) or Zn(II) facilitates its oxidation to the phenoxyl radical. This effect has been observed previously for Cu(II) complexes by Halcrow *et al.*[31] One mechanism for the stabilisation of the phenoxyl radical could involve back-donation, from metal d-orbitals into an empty π-orbital of $L^{\bullet}$. Such facilitation of phenoxyl radical formation presumably assists the formation of the tyrosinyl radical required for the active form of GAO.

The Cu(II)-phenoxyl radical complex, $[\mathbf{1}]^{+}$, possesses a diamagnetic ($S = 0$) ground state that is considered to arise from antiferromagnetic coupling between the unpaired electron of the Cu(II) and that of the coordinated phenoxyl radical, $L^{\bullet}$. However, this coupling ($|J| = 6.1$ cm^{-1}) is weak compared to that observed for the Cu(II)-tyrosinyl radical pair of the active form of GAO ($|J| > 200$ cm^{-1}).[32] This strong antiferromagnetic interaction has been rationalised by a qualitative magnetostructural model based on the Goodenough–Kananmori rules that proposes a significant overlap between the two half-occupied orbitals, *viz*. the Cu(II) $d_{x^2-y^2}$ and a π-orbital of the phenoxyl radical ligand.[33] The weak antiferromagnetic coupling in $[\mathbf{1}][BF_4]$ may imply that the orbital containing the unpaired electron on the Cu(II) centre and the half occupied π-orbital of the phenoxyl radical do not overlap effectively.

As for **1**, the Cu(II) centre of $[\mathbf{1}][BF_4]$ possesses a *cis*-arrangement of the two phenol *O*-donor atoms with the two 4,5-di-phenyl imidazole units being accommodated on the same side of the complex. Associated with this observation, $[\mathbf{1}]^{+}$ involves two intramolecular π–π interactions, between the phenyl ring of one ligand and the phenol and/or imidazole ring of the other ligand (Fig. 14). These involve: (i) the phenyl ring [C(12)–C(17)] of L^{-} and the phenol (PhO/Ph interaction) and the imidazole (IM/Ph interaction) ring of $L^{\bullet}$ and (ii) the phenyl ring [C(12A)–C(17A)] of $L^{\bullet}$ and the phenol (PhO/Ph) and the

Table 5 Geometrical parameters for the π–π stacking interactions in [**1**]·[BF_4]·2CH_2Cl_2, **1**·4DMF, **1**·3MeOH and **2**·[BF_4]·2CH_2Cl_2·0.75pentane

Compound	Interaction	Angles between P_{Ph} and P_{IM}/°	$dc_{IM}c_{Ph}$/Å	$dc_{IM}P_{Ph}$/Å	Offset Ph/IM/Å	Angles between P_{Ph} and P_{IM}/°	$dc_{PhO}c_{Ph}$/Å	$dc_{PhO}P_{Ph}$/Å	Offset PhO/Ph/Å	Angles between PhO and IM/° L	L(A)
[**1**]·[BF_4]·2CH_2Cl_2	Ph/IM(A)	6.4	3.43	3.29	0.99						
	Ph(A)/IM	9.5	3.51	3.30	1.11						
	Ph/PhO(A)					8.1	4.89	3.50	3.42		
	Ph(A)/PhO					9.9	4.69	3.60	3.01		
										2.3	8.3
1·4DMF	Ph/IM(A)	25.0	3.62	3.40	1.26						
	Ph(A)/IM	25.0	3.62	3.40	1.26						
	Ph/PhO(A)					12.8	5.57	2.50	4.96		
	Ph(A)/PhO					12.8	5.57	2.50	4.96		
										18.9	18.9
1·3MeOH	Ph/IM(A)	12.5	3.51	3.46	0.58						
	Ph(A)/IM	14.6	3.69	3.52	1.11						
	Ph/PhO(A)					17.0	4.54	3.65	2.70		
	Ph(A)/PhO					14.0	4.24	3.65	2.14		
										18.9	15.2
2·[BF_4]·2CH_2Cl_2·0.75pentane	Ph/IM(A)	9.6	3.78	3.60	1.15						
	Ph/PhO(A)					6.7	4.34	3.24	2.89		
										15.7	12.2

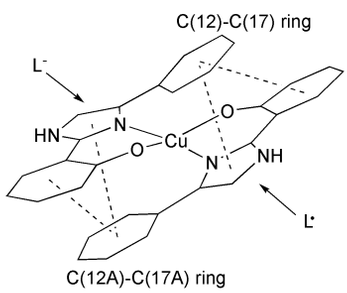

Fig. 14 View of [**1**]$^+$ in [**1**][BF_4]·2CH_2Cl_2 showing the intramolecular π–π interactions between the two ligands L^A ($L^{\bullet}$) and L^B (L^-). For each ligand, one phenyl ring and the two ^{t}Bu groups have been omitted for clarity.

imidazole (IM/PhO) ring of L^- (Fig. 14). Values of the parameters (Fig. 15) used to describe these interactions (Table 5) are in the range observed for graphitic interactions between two arene rings.[34]

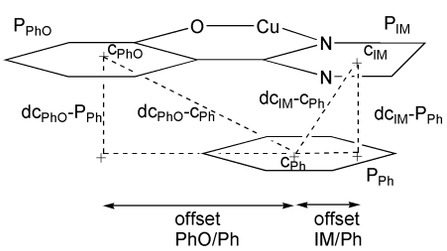

Fig. 15 A representation of the parameters involved in the interactions PhO/Ph and IM/Ph in [**1**]$^+$ and [**2**]$^+$. The letter c is used for centroid of a ring and P for plane.

Similar π–π interactions are observed for **1** in **1**·4DMF and **1**·3MeOH (Table 5). The presence of these π–π interactions are consistent with the *cis*-structures observed for the Cu(II) centres of **1**·4DMF, **1**·3MeOH, and [**1**][BF_4]·2CH_2Cl_2.

Although the distorted square planar geometry of the Cu(II) centres of **1** and [**1**]$^+$ allows the intramolecular interligand π–π interactions described above, this is not the case for the tetrahedral centre of **2**. However, in [**2**]$^+$ there is π–π interaction between the phenyl ring of L^- [C(12)–C(17)] and the phenol/imidazole system of $L^{\bullet}$ (Fig. 16, Table 5). Thus, in [**2**]$^+$, the twist angle between the C(12)–C(17) plane and the imidazole plane (75.5°) in the ligand L^- is significantly *larger* than that in $L^{\bullet}$ (42.0°) and that in both of the ligands in **2** [42.7° for L and 27.3° for L(A)]. Thus, oxidation of **2** to [**2**]$^+$ leads to a twist of the C12–C17 ring that orients this ring parallel to the plane of the phenol/imidazole unit of $L^{\bullet}$. The values obtained for the interactions C(12)–C(17)/PhO(A) [Ph/PhO(A)] and [C(12)–C(17)]/IM(A) [Ph/IM(A)] (Figs. 15 and 16; Table 5) resemble those obtained for graphitic interactions between two arenes.[34]

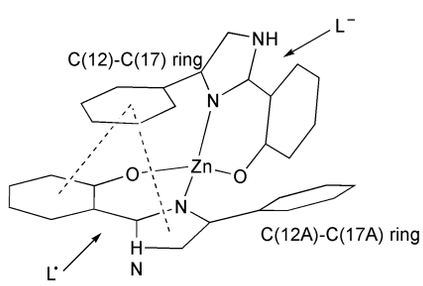

Fig. 16 View of [**2**]$^+$ in [**2**][BF_4]·2CH_2Cl_2·0.75 pentane showing the intramolecular π–π interactions between the C(12)–C(17) ring of L^B(L^-) and the phenol–imidazole unit of L^A($L^{\bullet}$). For each ligand, one phenyl ring and the two ^{t}Bu groups have been omitted for clarity.

Thus, in [**1**]$^+$ and [**2**]$^+$ the phenoxyl radical ligand is involved in intramolecular π–π stacking interactions. These interactions mimic the stacking of Tyr272 above the Trp290 indole ring[3] in the active site of GAO that has been suggested to contribute to the unusual stability of the phenoxyl radical of the catalytically active form of GAO.[35] However, the significance of this interaction has been debated by Halcrow[36] and Liu *et al.*[37] have shown that, for 1-{pyrid-2-yl}-3-{2′,5′-dimethoxyphenyl}-pyrazole radical complexes of Cu^{II}, intramolecular π–π stacking has no measurable effect on their kinetic stability. The results reported herein represent the first structural characteris-

ation of phenoxyl radical complexes involving π–π stacking interactions that parallel those observed in GAO. As noted above, these interactions may well lower the oxidation potential of the ligand and assist the formation of L$^{\bullet}$, however, the kinetic and/or thermodynamic effects engendered by the π–π stacking interactions have yet to be established.

Acknowledgements

We thank the EPSRC for provision of financial support, the University of Nottingham for the provision of a studentship (to L. B.) and Dr F. E. Mabbs and Professor M. W. George for valuable discussions.

References

1 J. W. Whittaker, in *Metal Ions in Biological Systems*, H. Sigel and A. Sigel, eds., Marcel Dekker, New York, 1994, vol. 30, pp. 315–360.
2 J. P. Klinman, *Chem. Rev.*, 1996, **96**, 2541.
3 (*a*) N. Ito, S. E. V. Phillips, C. Stevens, Z. B. Ogel, M. J. McPherson, J. N. Keen, K. D. S. Yadav and P. F. Knowles, *Nature*, 1991, **350**, 87; (*b*) N. Ito, S. E. V. Phillips, K. D. S. Yadav and P. F. Knowles, *J. Mol. Biol.*, 1994, **238**, 794.
4 (*a*) M. M. Whittaker, P. J. Kersten, N. Nakamura, J. Sanders-Loehr, E. S. Schweizer and J. W. Whittaker, *J. Biol. Chem.*, 1996, **271**, 681; (*b*) M. M. Whittaker, P. J. Kersten, D. Cullen and J. W. Whittaker, *J. Biol. Chem.*, 1999, **274**, 36226.
5 L. Benisvy, A. J. Blake, D. Collison, E. S. Davies, C. D. Garner, E. J. L. McInnes, J. McMaster, G. Whittaker and C. Wilson, *Chem. Commun.*, 2001, 1824.
6 J. Cosier and A. M. Glazer, *J. Appl. Crystallogr.*, 1986, **19**, 105.
7 (*a*) G. M. Sheldrick, SHELX-86-97, *Acta Crystallogr., Sect. A*, 1990, **46**, 467; (*b*) M. N. Burnett and C. K. Johnson, ORTEP-III: Oak Ridge Thermal Ellipsoid Plot Program for Crystal Structure Illustrations, Report ORNL-6895, Oak Ridge National Laboratory, Oak Ridge, TN, USA, 1996.
8 C. Foces-Foces, A. L. Llamas-Saiz, R. M. Claramunt, P. Cabildo and J. Elguero, *J. Mol. Struct.*, 1998, **440**, 193.
9 F. H. Allen, O. Kennard, D. G. Watson, L. Brammer, A. G. Orpen and R. Taylor, *J. Chem. Soc., Perkin. Trans. 2*, 1987, S1.
10 J. Catalan, F. Fabero, M. Soledad Guijarro, R. M. Claramunt, M. D. Santa Maria, M. C. Foces-Foces, F. H. Cano, J. Elguero and R. Sastre, *J. Am. Chem. Soc.*, 1990, **112**, 747.
11 A. L. Llamas-Saiz, C. Foces-Foces, D. Sanz, R. M. Claramunt, J. Dotor, J. Elguero, J. Catalan and J. C. del Valle, *J. Chem. Soc., Perkin. Trans. 2*, 1995, 1389.
12 R. H. Holm and M. J. O'Connor, *Prog. Inorg. Chem.*, 1971, **14**, 241.
13 (*a*) H. Sakiyama, H. Okawa, N. Matsumoto and S. Kida, *J. Chem. Soc., Dalton. Trans.*, 1990, 2935; (*b*) T. Sogo, J. Romero, A. Sousa, A. de Blas, M. L. Duran and E. E. Castellano, *Z. Naturforsch., Teil B*, 1988, **43**, 611; (*c*) E. Frasson and C. Panattoni, *Z. Kristallogr.*, 1961, **116**, 154.
14 (*a*) C. Bolm, K. Weickhardt, M. Zehnder and D. Glasmacher, *Helv. Chim. Acta*, 1991, **74**, 717; (*b*) J. D. Crane, E. Sinn and B. Tann, *Polyhedron*, 1999, **18**, 1527.
15 F. E. Mabbs and D. Collison, *Electron Paramagnetic Resonance of d-Transition Complexes*, Elsevier, Amsterdam, 1992, p. 405.
16 F. E. Mabbs and D. Collison, *Electron Paramagnetic Resonance of d-Transition Complexes*, Elsevier, Amsterdam, 1992, p. 218.
17 J. Peisach and W. R. Blumberg, *Arch. Biochem. Biophys.*, 1974, **165**, 691.
18 B. A. Jazdzewski and W. B. Tolman, *Coord. Chem. Rev.*, 2000, **200**, 633.
19 R. H. Holm, G. W. Everett Jr and A. Chakravorty, *Prog. Inorg. Chem.*, 1966, **7**, 83.
20 (*a*) J. A. Halfen, B. A. Jazdzewski, S. Mahapatra, L. M. Berreau, E. C. Wilkinson, L. Que Jr and W. B. Tolman, *J. Am. Chem. Soc.*, 1997, **119**, 8217; (*b*) E. Bill, J. Müller, T. Weyhermüllller and K. Wieghardt, *Inorg. Chem.*, 1999, **38**, 5795; (*c*) A. Sokolowski, J. Müller, T. Weyhermüllller, R. Schnepf, P. Hildebrant, K. Hildenbrand, E. Bothe and K. Wieghardt, *J. Am. Chem. Soc.*, 1997, **119**, 8889.
21 A. Sokolowski, E. Bothe, E. Bill, T. Weyhermüllller and K. Wieghardt, *Chem. Commun.*, 1996, 1671.
22 (*a*) E. R. Altwicker, *Chem. Rev.*, 1967, **67**, 475; (*b*) E. J. Land, G. Porter and E. Strachan, *Trans. Faraday Soc.*, 1961, **57**, 1885; (*c*) E. J. Land and G. Porter, *Trans. Faraday. Soc.*, 1963, **59**, 2016.
23 T. Maki, Y. Araki, Y. Ishida, O. Onomura and Y. Matsumura, *J. Am. Chem. Soc.*, 2001, **123**, 3371.
24 T. A. Gadosy, D. Shukla and L. J. Johnston, *J. Phys. Chem. A*, 1999, **103**, 8834.
25 O. Hammerich, in *Organic Electrochemistry*, M. M. Baizer and H. Lund, eds., Marcel Dekker, New York, 1983, p. 485.
26 A. B. Suttie, *Tetrahedron Lett.*, 1969, **12**, 953.
27 (*a*) O. Hammerich, V. D. Parker and A. Ronlan, *Acta Chem. Scand., Ser. B*, 1976, **30**, 89; (*b*) A. Nilsson, U. Palmquist, A. Ronlan and V. D. Parker, *J. Am. Chem. Soc.*, 1975, **97**, 3540; (*c*) U. Svanholm, K. Bechgaard and V. D. Parker, *J. Am. Chem. Soc.*, 1974, **96**, 2409.
28 (*a*) D. A. Force, D. W. Randall, R. D. Britt, X. S. Tang and B. A. Diner, *J. Am. Chem. Soc.*, 1995, **117**, 12643; (*b*) K. A. Campbell, J. M. Peloquin, B. A. Diner, X. S. Tang, D. A. Chisholm and R. D. Britt, *J. Am. Chem. Soc.*, 1997, **119**, 4787.
29 J. McMaster, R. L. Beddoes, D. Collison, D. R. Eardley, M. Helliwell and C. D. Garner, *Chem. Eur. J.*, 1996, **2**, 685.
30 (*a*) P. F. Knowles, R. D. Brown, S. H. Koenig, S. Wang, R. A. Scott, M. A. McGuirl, D. E. Brown and D. M. Dooley, *Inorg. Chem.*, 1995, **34**, 3895; (*b*) K. Clark, J. E. Penner-Hahn, M. M. Whittaker and J. W. Whittaker, *Biochemistry*, 1994, **33**, 12553; (*c*) K. Clark, J. E. Penner-Hahn, M. M. Whittaker and J. W. Whittaker, *J. Am. Chem. Soc.*, 1990, **112**, 6433.
31 M. A. Halcrow, L. M. L. Chia, X. Liu, E. J. L. McInnes, L. J. Yellowlees, F. E. Mabbs, I. J. Scowen, M. McPartlin and J. E. Davies, *J. Chem. Soc., Dalton. Trans.*, 1999, 1753.
32 J. W. Whittaker and M. M. Whittaker, *Pure Appl. Chem.*, 1998, **70**, 903.
33 J. Müller, T. Weyhermüller, E. Bill, P. Hildebrandt, L. Ould-Moussa, T. Glaser and K. Wieghardt, *Angew. Chem., Int. Ed.*, 1998, **37**, 616.
34 (*a*) C. A. Hunter and J. K. M. Sanders, *J. Am. Chem. Soc.*, 1990, **112**, 5525; (*b*) C. Janiak, *J. Chem. Soc., Dalton. Trans.*, 2000, 3885.
35 C. G. Saysell, T. Barna, C. D. Borman, A. J. Baron, M. J. McPherson and A. G. Sykes, *J. Biol. Inorg. Chem.*, 1997, **2**, 702.
36 M. A. Halcrow, *Heteroatom. Chem.*, 2002, **13**, 494.
37 X. Liu, L. M. L. Chia, C. A. Kilner, L. J. Yellowlees, M. Thornton-Pett, S. Trofimenko and M. A. Halcrow, *Chem. Commun.*, 2000, 1947.
38 V. K. Mahesh, M. Maheshwari, R. Sharma and R. Sharma, *Can. J. Chem.*, 1985, **63**, 632.